# Remote Excitation of Hot Electrons via Propagating

# Surface Plasmons

Charlotte I. Evans<sup>1</sup>, Douglas Natelson<sup>1,2,3\*</sup>.

<sup>1</sup>Department of Physics and Astronomy, Rice University, Houston, TX 77005

<sup>2</sup>Department of Electrical and Computer Engineering, Rice University, Houston, TX 77005

<sup>3</sup>Department of Materials Science and NanoEngineering, Rice University, Houston, TX 77005

# ABSTRACT

Efficient hot electron generation in plasmonic nanostructures is of particular interest. Distinguishing between hot carrier generation and other competing effects due to direct absorption and heating can be challenging. Here, we report a study of the open-circuit photovoltage in thin-film gold nanostructures as a function of illumination position. Comparison is made between direct illumination of a nanowire constriction or electromigrated tunneling junction, and remote excitation via the use gratings in the surrounding electrode to excite propagating surface plasmon polaritons (SPPs). Photovoltage response in continuous nanowire constrictions is dominated by photothermoelectric effects, with grating illumination demonstrating that it is possible to achieve a nontrivial temperature distribution at the constriction due to SPP excitation. Direct illumination

of tunneling gaps had previously demonstrated enhanced photovoltages due to hot electron tunneling. We reconfirm this and find that the photovoltages generated by illuminating the gratings after electromigration are enhanced up to a factor of 100 compared to their pre-migration values. The polarization dependence and polarity of the signal with illumination at the grating provide evidence that the SPPs couple with local plasmon modes at the gap, producing hot electron current via plasmon decay, and a corresponding open-circuit voltage develops to enforce the open-circuit condition of no net current. Variations in such measurements show the sensitivity of SPP-local mode coupling to the structural details of the junctions.

#### Introduction

The generation of hot electrons in plasmonic structures is of great interest for applications such as energy conversion, sensing, and photochemistry<sup>1</sup>. It can be challenging, particularly in resonant structures, to disentangle the consequences of plasmonic hot carrier generation (from, e.g., the decay of localized surface plasmons or propagating surface plasmon polaritons (SPPs)) from competing effects, such as lattice and electron heating or the creation of electron-hole excitations due to direct absorption<sup>2</sup>. Prior experiments on atomic-scale junctions have shown evidence of plasmon-assisted transport, with possible roles of hot carriers<sup>3-8</sup>. Time-resolved pump-probe measurements have provided significant insight of the relaxation and thermalization of electrons and the heat dissipation of SPPs in plasmonic nanostructures<sup>1,9-15</sup>. Electron emission in the pulsed regime must additionally distinguish between conventional photoemission and strong plasmon-based fields<sup>16-19</sup>. However, many applications of interest for hot carrier generation likely require continuous illumination, such as photocatalysis and solar energy conversion.

Previous experiments<sup>20-23</sup> in nanowire constrictions under focused illumination have shown photothermoelectric response. The spatial variation in conductor geometry leads to a corresponding spatial dependence of the local Seebeck coefficient due to the effects of boundary scattering on electronic mean free path<sup>24</sup>. The junction between the nanowire and the larger electrodes functions as an effective thermocouple. The open-circuit photovoltage (OCPV) develops to counteract the diffusion of charge carriers driven by the local temperature gradient. OCPV measurements are comparatively immune to some confounding effects that can result in measurements of photocurrents, such as temperature-dependent variations in device conductance or thermal expansion-related distortions of device geometry. In gold constrictions, OCPVs on the order of a microvolt per mW incident power are consistent with expected Seebeck variation and local temperature gradients<sup>23, 25</sup>.

Direct illumination of electromigrated tunneling nanojunctions has shown OCPVs that are orders of magnitude larger, reaching mV/mW incident power<sup>23</sup>. These are consistent with the generation of hot electron photocurrents<sup>26-27</sup>. In an open-circuit configuration in steady state, a DC potential difference will develop between the two sides of the junction such that ordinary tunneling current will counterbalance any net hot electron current. The open-circuit configuration provides several advantages to distinguishing between the generation of hot carriers and other competing effects (e.g., thermal expansion resulting in changes in the interelectrode conductance; thermoelectric currents)<sup>23, 28</sup>. While the pulsed retime has provided insight in some experiments<sup>13</sup>, in prior OCPV measurements it was not possible to distinguish between hot carriers produced by plasmonic decay processes<sup>29</sup> and those produced by direct optical absorption. We note that the production of hot carriers near some tunneling gap is not sufficient to produce hot electron currents. Hot carrier tunneling requires production of carriers with both appropriate energy and momentum

distributions<sup>30-33</sup>, and these depend on the particular relevant plasmon modes. Disorder (grain boundaries, rough surfaces) can relax conservation of crystal momentum, further making hot carrier production and tunneling sensitive to structural details.

Optical energy may be delivered to a nanoscale tunneling gap via the spatially remote excitation of propagating SPPs. Gratings to break the translational symmetry of the source or drain electrodes have proven effective at facilitating such excitation<sup>5, 34-37</sup>. SPP excitations in metallic nanoconstrictions and point contacts have been electronically detected both in the steady-state<sup>38-39</sup> and in the pulsed regime<sup>6-7, 40</sup>. Indirect detection of SPPs based on differential conductance measurements of atomic point contacts and nanoconstrictions paired with modeling have shown that SPPs can deliver energy to a nanowire constriction with a local temperature increase nearly two orders of magnitude smaller than the direct illumination case<sup>34</sup>.

Here we report a study of OCPVs generated by grating-based remote excitation of nanowire constrictions and tunneling nanogaps under continuous illumination. The SPPs are launched using gratings fabricated at various distances from the nanowire constriction in the electrode design. Illuminating these gratings when the nanowire is intact results in a nonuniform temperature distribution across the constriction, resulting in OCPVs that can be explained using conventional thermoelectric effect physics. Electromigrating the nanowire to create a gap at the nanoscale causes large enhancements of the open circuit voltage signal not only when the nanogap is directly illuminated, but also when light is focused on the gratings. By studying the polarization dependence of the open circuit voltage at both the gratings and at the nanogap, we find that details of how the SPPs interact with the local plasmonic modes of the nanogap can be electronically detected without the use of optical detection. These measurements show that propagating SPPs can couple into various local plasmon modes of the nanogap, resulting in asymmetric hot electron

tunneling across the gap. The device-to-device variability of the OCPV response shows the sensitivity of the SPP-local mode coupling to the fine details of the structures.

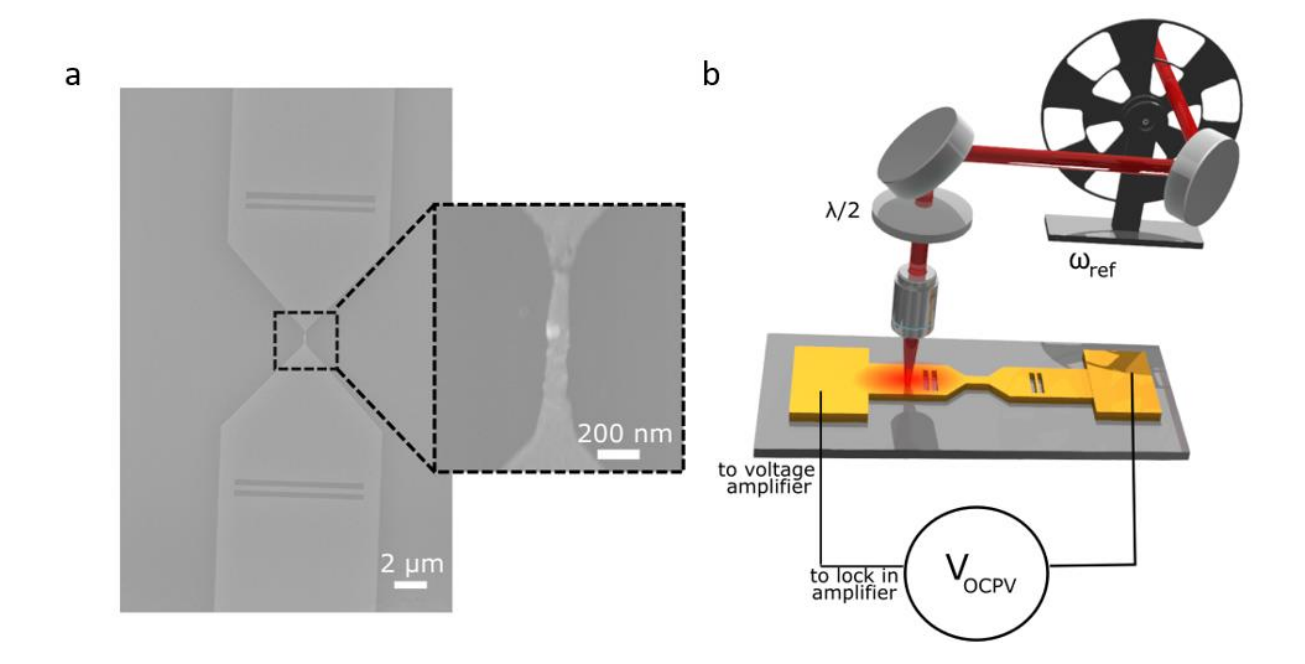


**Figure 1**: a. Scanning electron micrograph of a typical device. The angle defines the orientation of the electric field of the polarized incident radation, with 0°, the longitudinal orientation, defined as parallel to the length of the device. Inset: SEM image of the electromigrated junction. b. Schematic of experimental setup

The devices in this work are fabricated on a silicon substrate with 2 µm thermal oxide, and comprise lithographically defined 30 nm thin film gold structures, each consisting of a nanowire between two fan-out electrodes which extend to larger pads for wire bonding, Fig. 1a. An ensemble of 22 devices was measured. In the electrode design, two rectangular slots ("gratings") on either side of the constriction were placed at six different distances from the constriction. The distances chosen between the center of the slots and the center of the constriction were uniformly

spaced between 5.2  $\mu$ m and 10.2  $\mu$ m for the various different devices examined. The device geometry is discussed further in previous work<sup>34</sup> and in Experimental Details. Prior to electromigration of the nanowire, the steady state, integrated open circuit photovoltage (OCPV) as a function of laser position was measured using a focused, raster-scanning 785 nm CW laser diode as a heating source with a spot size diameter of 1.8  $\mu$ m, Fig. 1b. Lock-in detection isolates the signal produced purely due to the photoexcitation. The optical chopper timescale (milliseconds) is far longer than the thermal equilibration timescale of the metal nanostructure, so that the measured response is essentially the thermal steady state. This experimental approach is discussed in previous publications<sup>23, 25, 41</sup>. In a one dimensional model, the OCPV of a device of length l, with both ends kept at a constant, uniform temperature, while the laser heats the device somewhere in the middle, is  $V = \int_0^l S(x, T)\nabla T(x)dx$ , where x is the distance along the device, S(x, T) is the Seebeck coefficient of the material, which is both temperature and position dependent, and T(x) is the local temperature. Unless otherwise indicated, measurements were taken with the substrate in vacuum (< 10.5 mB) and at room temperature (~ 298 K).

# **Results and Discussion**

The spatial maps of the integrated OCPV as a function of laser position with an intact nanowire are seen in the first column of Fig. 2a. In these maps, the incident polarization is in the longitudinal orientation ( $\theta = 0^{\circ}$ ) to favor excitation of SPPs from the gratings. The middle panel shows the OCPV spatial map of the intact nanowire and the surrounding fan-out electrodes. At the nanoscale, the Seebeck coefficient is sensitive to changes of the electron mean free path. The change in metal geometry at the connection between the fan-out electrodes and the nanowire constriction causes a

local change in the S, an effective thermocouple<sup>24</sup>. The sign of the resulting photothermoelectric voltage correspondingly depends on the sign of the local temperature gradient, resulting in a change of OCPV polarity as the laser heat source traverses from one side of the constriction to the other. The OCPV signal is very position sensitive, even within the spot size of the laser, with the maximum signal occurring at the nanowire/electrode interface. The polarization dependence of the OCPV with the laser spot at this location is seen to the right. The OCPV signal is slightly larger when the laser polarization in the transverse ( $\theta = 90^{\circ}$ ) orientation, which agrees with previous results<sup>23, 42</sup>. This polarization dependence originates from a transverse plasmon resonance in the nanowire that depends on nanowire width and thickness<sup>43</sup>. The signal is normalized to the incident power as the relationship between the two is linear, SI Figs. 1 and 2.

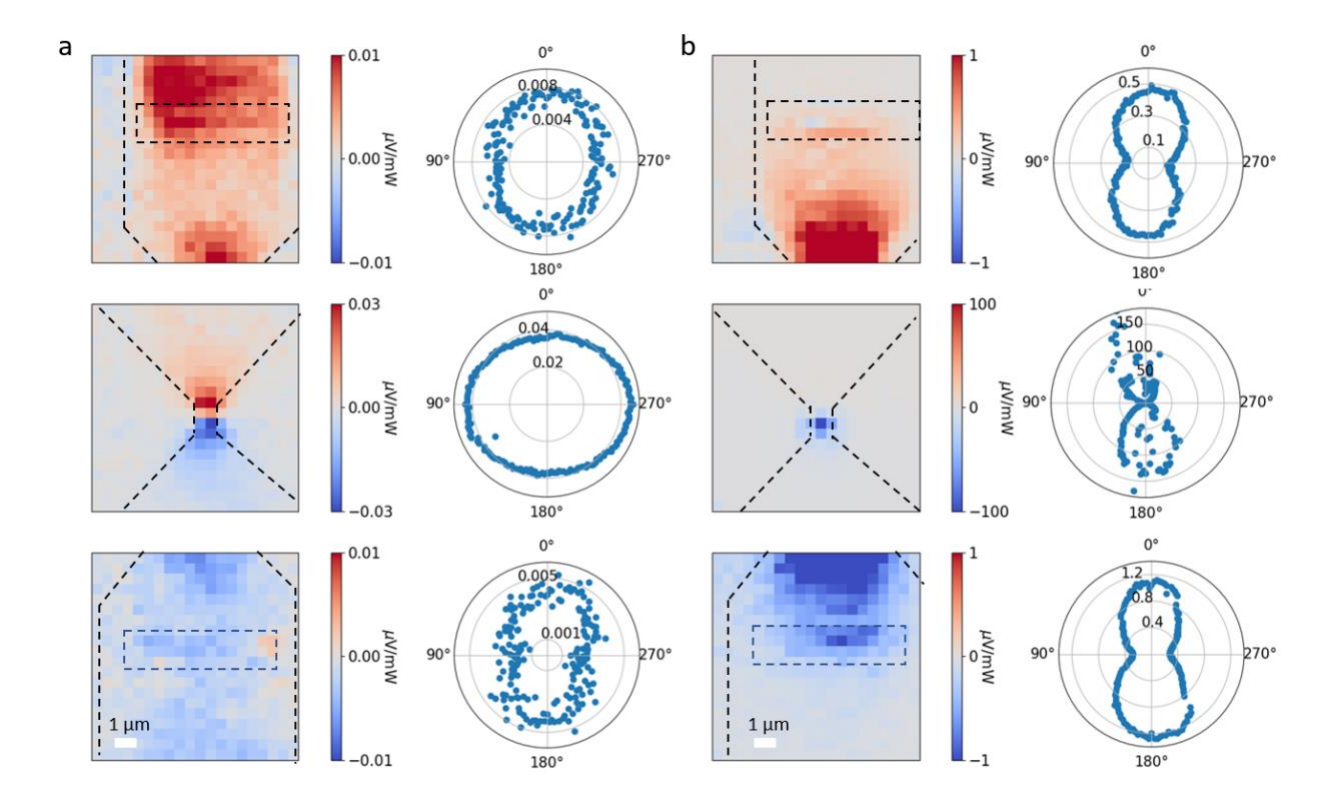


**Figure 2**: a. OCPV spatial maps and polarization dependence of a device before electromigration, with a continuous Au nanowire constriction. Sample boundaries and grating locations are indicated by dashed lines. In all spatial maps, the ground is connected to the bottom electrode. Top panel: OCPV signal when the device's top grating is measured. The polarization dependence of the signal at the grating agrees with the excitation of SPPs. Middle panel: OCPV signal just on one side of the constriction when the unbroken nanowire and surrounding electrodes are measured. The polarization dependence is consistent with expectations of a transverse plasmon resonance in the nanowire<sup>42-43</sup>. Bottom panel: OCPV signal when the bottom grating is measured. The polarization dependence of the signal at the grating agrees with the excitation of SPPs.

b. OCPV spatial maps and polarization dependence of the device in Fig. 2a after electromigration to a resistance of  $100 \text{ k}\Omega$ . The signal under direct illumination of the nanogap region becomes  $3000\times$  larger than the premigration value but is highly localized to the nanogap. The signal for illumination at the gratings increases by  $100\times$  relative to the premigration value. In all cases, the polarization dependence of the OCPV response becomes much more pronounced.

The top and bottom panels of the same column show the OCPV spatial maps of the gratings placed 10.2 and 9.2 µm from the constriction, respectively. While there is more OCPV signal when the laser is incident on the gratings, the signal is relatively weak, around twice the signal when the laser is incident on the gold but away from any feature. The polarization dependence of the OCPV while the light is incident on the grating has the same signature as the grating-based excitation of SPPs<sup>5, 35</sup>. The average temperature rise of the constriction due to remote SPP excitation from gratings at these distances and illumination conditions for this device geometry was calculated to

be around 0.3 K<sup>34</sup>. This relatively weak OCPV signal with the laser incident on the grating, paired with the polarization dependence, indicates that the excited SPPs remotely heat the constriction, resulting in a *nonuniform* temperature distribution across the constriction and a corresponding photothermoelectric response. The OCPV response depends on the spatial asymmetry of this small temperature perturbation across the constriction.

Electromigrating the devices to resistances above the quantum resistance ( $h/2e^2 \approx 12.9 \text{ k}\Omega$ ) creates a gap within the nanowire and results in significant changes in the OCPV spatial maps, Fig. 2b. The middle panel of the shows the OCPV spatial map and polarization dependence when the nanogap is directly illuminated. Unlike the unbroken case, the OCPV signal is highly localized to the constriction and is detectable with only one voltage sign. The signal is also 3000× larger in this localized spot than the signal measured prior to breaking. As discussed previously<sup>23</sup>, this enhancement of the OCPV signal cannot be explained solely using traditional thermoelectric response. The Seebeck coefficient of tunnel junctions<sup>44</sup> and molecular junctions<sup>3, 45-46</sup> is typically  $\sim 10 \mu V/K$ , and that of atomic-scale metal junctions is even smaller<sup>47</sup>. These would yield significantly smaller photovoltages for reasonable temperature distributions from illumination. There is no reason to expect an enormous increase in Seebeck response or large change in the temperature distribution in the electrodes. Instead, the large photovoltages at the gap are thought to occur to counteract the current from the hot electron tunneling across the gap<sup>23, 27</sup>. Optically generated hot carriers relax on the timescale of 10s to 100s of fs, and thus are only a small perturbation on the electronic distribution under steady-state illumination<sup>27</sup>. However, estimates<sup>26</sup>, <sup>48</sup> show that these are sufficient to contribute detectable hot electron currents  $I_{he}$ ; in an open-circuit configuration, an OCPV must develop to offset any net  $I_{he}$ ,  $V_{oc} = I_{he} / (dI/dV)$ , where (dI/dV) is the zero-bias tunneling conductance<sup>27</sup>.

The single polarity of the OCPV signal indicates that there is some asymmetry between the two sides of the gap in terms of hot electron generation and tunneling. Illumination of the nanogap region generates hot carriers through both direct absorption and excitation and decay of local plasmon modes. If hot carriers are generated with equal efficiency and momentum distributions on both sides of the nanogap, and tunneling transmission is equally probable in both directions, then no hot carrier OCPV signal would be expected, as illumination would not produce a net hot electron current. The symmetry routinely seen in the junction current-voltage curves indicates that the transmission probability between the source and drain are nearly identical, at least at bias energy scales near the Fermi level, SI Fig. 3. The observation of a single dominant polarity of OCPV, a very common occurrence in these electromigrated nanogaps, then likely originates with asymmetry in the generation of hot carriers able to tunnel from one side of the nanogap to the We emphasize that this asymmetry must originate from the efficiency with which the particular local plasmon modes are excited and produce hot carriers with appropriate energy and momentum distributions for tunneling<sup>30-33</sup>. The strong polarization dependence of the OCPV signal at the nanogap provides supporting evidence that this process is enhanced by the resonant coupling of plasmonic modes, known to create populations of relatively long-lived hot electrons which can tunnel across the gap<sup>1</sup>.

The polarization scan shows some instability as a function of time during the measurement, which indicates atomic-scale local changes in the tunneling geometry upon incident excitation, typical for electromigrated junctions at room temperature. Additionally, the polarization dependence varies strongly from device to device. Out of 22 devices in the ensemble, 7 had the dominant signal with the transverse polarization ( $\theta$ = 90°), consistent with prior results<sup>23</sup> obtained in structures with thinner (~15 nm) gold films. The remaining devices had a similar polarization dependence for

illumination at the nanogap shown in Fig. 2b. This suggests that the local details of the nanogap itself result in highly localized plasmon modes "built" from competing modes, including the longitudinal "lightning rod" mode, the transverse plasmons of the nanowire, and the hybridization of higher order multipolar modes due to symmetry breaking. This is consistent with prior observations in photocurrent measurements on related structures<sup>49</sup>. A scatter plot of the maximum signal at nanogap after electromigration vs. resistance after electromigration is seen in SI Fig. 4.

The OCPV signal when the laser spot is at the gratings, top and bottom panels of Fig. 2b, is similarly enhanced, by around a factor of 100 after electromigration. The strong polarization dependence of the OCPV signal confirms that efficient SPP excitation via the gratings is the origin of this signal. As with the large enhancement of the OCPV when the junction is directly illuminated, this coincident enhancement of the OCPV upon migration for grating illumination indicates that the propagating SPPs are coupling with the local modes of the nanogap and generating hot electrons, which can then tunnel across the gap. There is no credible change in temperature distribution or local Seebeck response that could lead to such an enhancement, and only some SPP/local mode coupling can be generating the hot carriers, as there is no direct absorption at the nanogap when the gratings are illuminated. As explained below, evidence indicates that the dominant source of hot carriers is from the local plasmon modes rather than directly from the propagating SPPs<sup>6</sup>. Previous studies have discussed the thermal expansion from SPP excitation in atomic scale junctions<sup>13, 40</sup>. Thermal expansion from SPPs can change the local geometry of the nanogap, resulting in nonzero differential conductance at zero bias which cannot result in a zero-bias photocurrent or open circuit photovoltage.

The scenario supported by the data is the following. The nanogap region supports localized plasmon excitations that are complicated, and involve<sup>50</sup> hybridization between the usual

interelectrode longitudinal mode (analogous to the tip plasmon in scanned probe geometries), the dipole-active transverse mode of the gold nanowire (resonant near 785 nm), and higher order multipolar modes localized to the gap ("dark" in the absence of symmetry breaking that allows coupling to the transverse plasmon). These modes may be excited with varying efficiencies via far-field direct illumination, and are responsible for the large local field enhancements used in surface-enhanced spectroscopies in these structures. Some of these modes, sensitive to specific structural details of particular junctions, can produce hot carriers with energy and momentum distributions that favor hot electron tunneling. The highly localized character of these modes and their dependence on structural details leads to asymmetries in such hot carrier tunneling, explaining why direct illumination often leads to a OCPV with one dominant sign and a polarization dependence associated with far-field excitation of the dominant mode(s).

Illumination at the gratings can excite propagating SPPs. These propagating SPPs can themselves create hot carriers during propagation and at the nanogap. These propagating SPPs can also couple to the localized modes at the gap, with efficiencies that would depend on the particular local modes. Hence any hot electron OCPV should have a polarization dependence dominated primarily by the coupling to the gratings (maximum signal with longitudinal polarization), and a sign set by the hot carrier asymmetry of the local mode(s) that couple most efficiently to the propagating SPPs.

The OCPV for the illumination at the gratings can change polarity after electromigration relative to the before-migration continuous nanowire situation. Fig. 3 presents two ways that this can take place. Fig. 3a shows a device in which the OCPV for illumination of the bottom grating before electromigration did not match the polarity as the OCPV generated in the same device when the nanowire constriction is illuminated on the same side. For this particular device, the grating was unusually close to the large contact pads (within 6  $\mu$ m), and the junction between the electrodes

and the large contact pads can also function as a thermocouple. Given the photothermoelectric origins of the OCPV in unmigrated constrictions, the polarity implies that when the device was unbroken, in addition to the SPPs generated by that grating propagating toward the constriction, SPPs also propagated away from the device and instead heated the electrode/contact pad boundary, resulting in a contribution to the OCPV of the opposite polarity to, and larger than that of, the small contribution from the temperature gradient at the constriction. After electromigration, however, the signal from that grating changes polarity. The OCPV signal at that grating has the same polarity as when the nanogap is directly illuminated, indicating that the dominant signal now comes from the hot electron OCPV contribution from SPPs excited from the grating coupled with plasmonic modes in the nanogap.

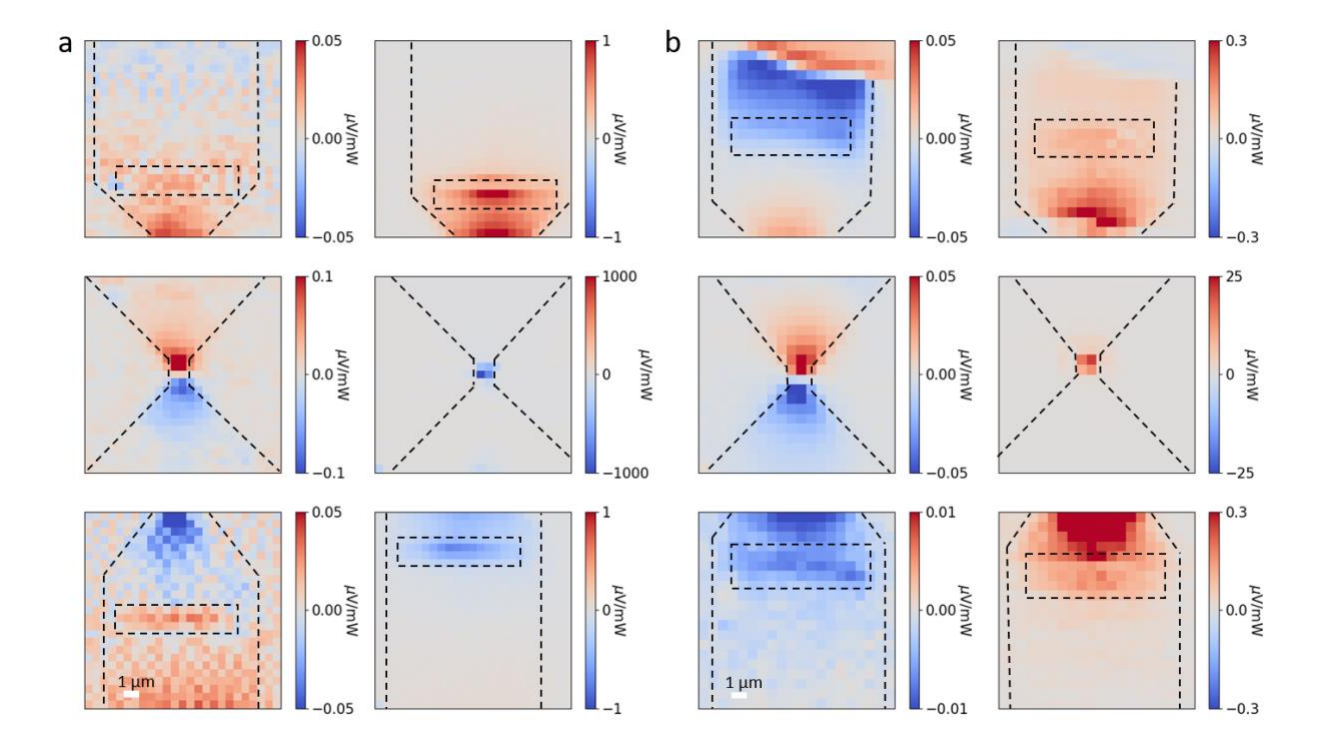


**Figure 3**: a. Left: OCPV spatial maps of a device before electromigration. The OCPV signal at the bottom grating is of opposite polarity compared to that of the constriction on the same side. The positive (red) voltage generated at the very bottom of the lowest panel results from photothermoelectric response of the junction between that electrode and the large contact pad. Right: OCPV spatial maps of the same device after electromigration. The signal at the bottom grating changes polarity after electromigration, showing that the hot electron contribution from SPPs interacting with the nanogap greatly exceeds any contribution from SPPs interacting with the contact pad.

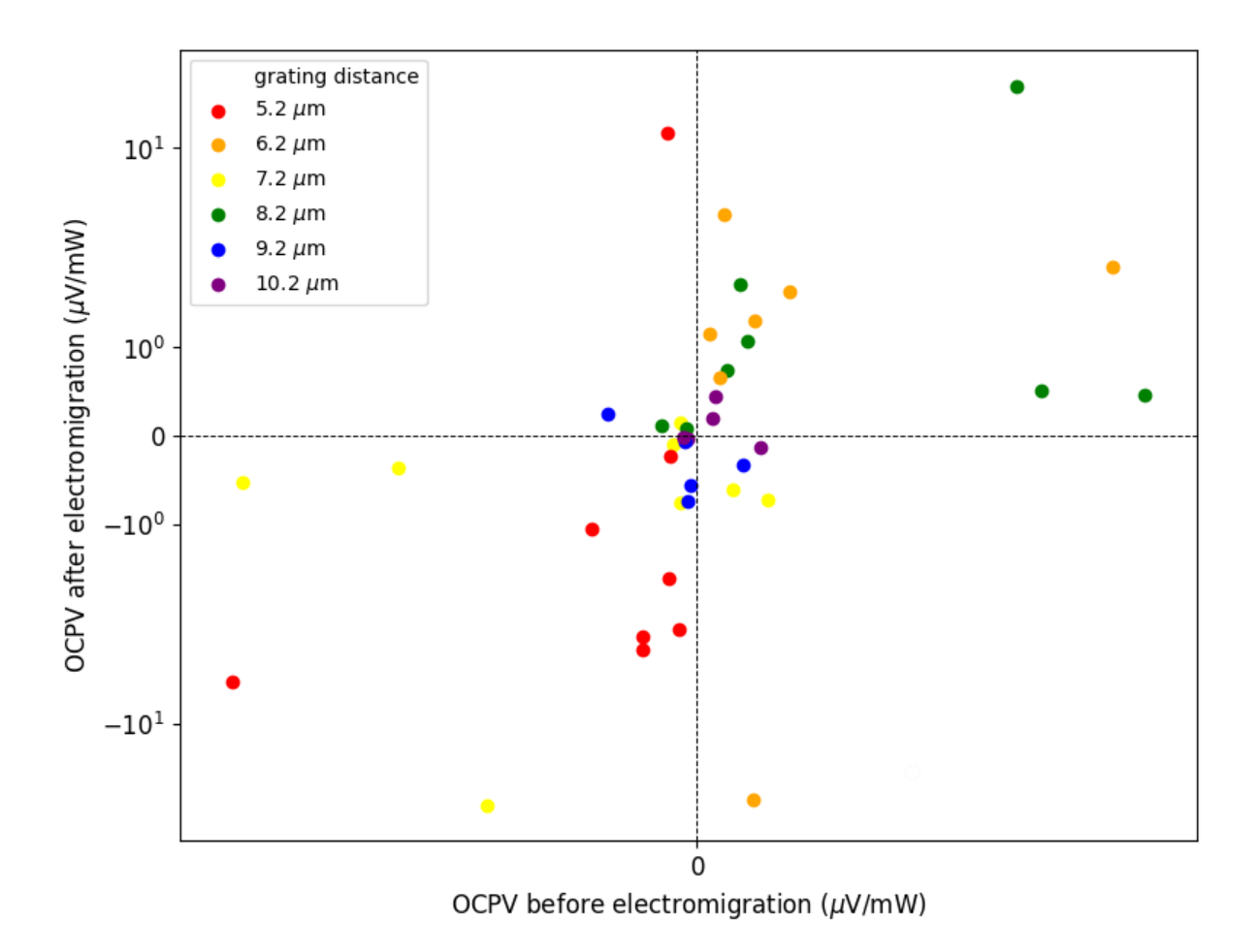
b. Left: OCPV spatial maps of a device before electromigration. The OCPV signal at the bottom grating has the same polarity compared to that of the constriction on the same side, while the top grating has the opposite polarity. In this case, SPPs from the top grating are interacting with the electrode/contact pad interface, readily apparent in the top panel. Right: OCPV spatial maps of the same device after electromigration. Both gratings have the same polarity, indicating asymmetric excitation of tunneling hot electrons at the nanogap.

Fig. 3b shows another device where the OCPV signal at the bottom grating changes polarity after breaking, but for a different, more interesting reason. In this device, it is the top grating that is close to the electrode/contact pad interface. As a result, illuminating the top grating produces a net OCPV signal that is opposite in polarity to that found when directly illuminating the upper part of the constriction. After electromigration, *both* gratings' signal change polarity to match that of the nanogap. The same sign of OCPV from illuminating both gratings implies that propagating SPPs arriving at the nanogap from *either* direction result in the current from hot electron generation

to flow in only one direction (in this case, electrons flowing toward the lower electrode). This surprising result indicates that SPPs propagating from either side couple to localized modes of the nanogap that produce *asymmetric* hot electron generation and tunneling. This is consistent with the scenario outlined above; it is inconsistent with the idea that the SPP propagation itself exclusively determines the momentum of hot carriers, and it is also inconsistent with any explanation in terms of thermal gradients due to SPPs incident on one side of the junction. This shows that the hot electron generation originates from local plasmon modes excited by the SPPs, not from the directionality of the SPPs themselves.

To visually represent the frequency of the occurrence of this asymmetric excitation of hot electron tunneling, Fig. 4 is a scatter plot of the OCPV signal at the grating after vs. before electromigration. The points in Quadrants I and III show gratings whose OCPV signal remained in the same polarity before and after electromigration. The points in Quadrants II and IV, however, show that 10 out of 42 gratings switched polarity after electromigration. A change in the signal polarity after electromigration is indicative of two things. As stated above, this demonstrates that SPPs are remotely exciting specific features of the device and are not simply resulting in asymmetric carrier generation based on the SPP propagation direction. Second, after electromigration the generated photovoltages can result in asymmetric hot carrier current that is counter to the direction of heating due to remote excitation, and counter to the direction of any temperature gradient due to heating at the gratings. Of those, 3 devices resulted in both gratings having the same sign of OCVP after electromigration. The plot also demonstrates the large device-to-device variability in hot electron OCPV response, despite comparatively similar conductivities after electromigration. This deviceto-device variability can be explained due to the exponential relationship of the resonance energy level and the effective electron temperature to the hot carrier current. Additionally, the specific

local geometry of the nanogap at the junction will affect the local plasmonic modes present, which may couple differently with the remotely excited propagating plasmons.



**Figure 4**: Log-log scatter plot of the OCPV signal at the grating after vs. before electromigration. Points in Quadrants I and III indicate gratings with signal did not change polarity after electromigration. Points in Quadrants II and IV indicate gratings with signal that did change polarity after electromigration.

# **Conclusions**

In this work, we use open circuit photovoltage measurements to detect remote excitation of a nanowire constriction with and without electromigration, to investigate the role of localized and propagating plasmon modes in hot electron generation. In unbroken nanowires, the propagating SPPs lead to a nonuniform temperature distribution across the nanowire constriction, causing a detectable OCPV as described by conventional thermoelectric effects. After electromigration, the open circuit voltages of the device with direct illumination on the constriction can increase by a factor of 1000 due to hot electron generation and tunneling. Remotely exciting the constriction using SPPs from gratings can result in open circuit voltage signal at the grating to increase by a factor of 100. These greatly enhanced OCPV signals are not quantitatively consistent with interpretation in terms of thermoelectric response, and instead are consistent with an OCPV arising to compensate hot electron tunneling. This signal provides insight to how the SPPs couple to the local modes of the nanogap to generate tunneling hot electrons. Despite comparatively similar electronic conduction characteristics, a great variety is seen in the magnitudes, local polarization dependences, and grating excitation efficiencies of hot electron OCPVs. This variation makes sense given the sensitive dependence of particular local plasmon modes<sup>50</sup> and generation of hot carrier energy and momentum distributions to microscopic structural features<sup>30-33</sup>. Detailed modeling of these effects is extremely demanding, requiring treatments of optical and plasmonic properties on scales from deep subwavelength to several wavelengths, as well as realistic treatments of the tunneling process. These measurements motivate such studies by showing the variation of the SPP/local plasmon coupling and the nontrivial asymmetry of plasmon-generated hot electron currents. Further studies to determine the optimized geometry for remote excitation

of hot electron production can provide insight on how to implement this mechanism for measurements that require low local temperatures at the nanogap. Time resolved measurements can further provide insight on how the SPPs remotely couple and asymmetrically excite hot electrons across the nanogap.

# **Experimental Details**

Devices were fabricated on p-type Si wafers with 2 μm SiO<sub>2</sub> thermally grown oxide. Before device fabrication, large Au pads with Ti adhesion layer for wire bonding were deposited using a shadow mask. The devices were then fabricated using a single step of electron beam lithography and depositing 30 nm Au/1 nm Ti. All metal deposition was completed using electron beam evaporation. Each sample consisted of 24 devices which shared a common ground. A total of 55 devices were studied for this work; the results in this paper demonstrate a typical device behavior. The steady state, open circuit voltage was measured using a home-built Raman system with a raster-scanning 785 nm CW laser diode. 20 mW of power was incident on the device with a focused diameter of 1.8 µm. The linear polarization of the incident light was rotated using a half wave plate. An optical chopper was used to modulate the light intensity and was as the reference signal for the lock-in amplifier. The chopper frequency was at 367 Hz, much slower than the thermalization timescale of the devices. The voltage at each of the leads was amplified using a SR560 voltage amplifier with the potential difference measured as the input of the lock-in amplifier. The devices were measured while under high vacuum in a closed-cycle Montana Instruments cryostat. All measurements in this work were conducted at room temperature.

**Supporting Information**. The supporting information contains figures showing the linearity of the OCPV as a function of incident optical power; example current/voltage and differential conductance data of a typical electromigrated junction; and scatter plots and histograms showing the wide variety of OCPV responses in devices and their correlations. The following files are available free of charge.

supporting evans grating ocpv.pdf (PDF)

AUTHOR INFORMATION

**Corresponding Author** 

\*natelson@rice.edu.

**Author Contributions** 

DN and CIE planned the series of experiments. CIE fabricated the devices and performed the measurements. DN and CIE analyzed and interpreted the data. The manuscript was written through contributions of both authors. Both authors have given approval to the final version of the manuscript.

**ACKNOWLEDGMENT** 

DN and CIE acknowledge support from Robert A. Welch Foundation Grant C-1636. DN acknowledges further support from NSF award ECCS-1704625.

**REFERENCES** 

- 1. Brongersma, M. L.; Halas, N. J.; Nordlander, P., Plasmon-Induced Hot Carrier Science and Technology. *Nat Nanotechnol* **2015**, *10*, 25.
- 2. Dubi, Y.; Sivan, Y., "Hot" Electrons in Metallic Nanostructures-Non-Thermal Carriers or Heating? *arXiv preprint arXiv:1810.00565* **2018**.
- 3. Vadai, M.; Nachman, N.; Ben-Zion, M.; Bürkle, M.; Pauly, F.; Cuevas, J. C.; Selzer, Y., Plasmon-Induced Conductance Enhancement in Single-Molecule Junctions. *The Journal of Physical Chemistry Letters* **2013**, *4*, 2811-2816.
- 4. Vadai, M.; Selzer, Y., Plasmon-Induced Hot Carriers Transport in Metallic Ballistic Junctions. *The Journal of Physical Chemistry C* **2016**.
- 5. Benner, D.; Boneberg, J.; Nürnberger, P.; Ghafoori, G.; Leiderer, P.; Scheer, E., Transmission of Surface Plasmon Polaritons through Atomic-Size Constrictions. *New J. Phys.* **2013**, *15*, 113014.
- 6. Benner, D.; Boneberg, J.; Nürnberger, P.; Waitz, R.; Leiderer, P.; Scheer, E., Lateral and Temporal Dependence of the Transport through an Atomic Gold Contact under Light Irradiation: Signature of Propagating Surface Plasmon Polaritons. *Nano Lett* **2014**, *14*, 5218-5223.
- 7. Guhr, D. C.; Rettinger, D.; Boneberg, J.; Erbe, A.; Leiderer, P.; Scheer, E., Influence of Laser Light on Electronic Transport through Atomic-Size Contacts. *Phys. Rev. Lett.* **2007,** *99*, 086801.

- 8. Kopp, B.; Yi, Z.; Benner, D.; Xie, F.-Q.; Obermair, C.; Schimmel, T.; Boneberg, J.; Leiderer, P.; Scheer, E., Revealing Thermal Effects in the Electronic Transport through Irradiated Atomic Metal Point Contacts. *Beilstein Journal of Nanotechnology* **2012**, *3*, 703-711.
- 9. Baffou, G.; Girard, C.; Quidant, R., Mapping Heat Origin in Plasmonic Structures. *Phys. Rev. Lett.* **2010**, *104*, 136805.
- 10. Baffou, G.; Quidant, R., Thermo-Plasmonics: Using Metallic Nanostructures as Nano-Sources of Heat. *Laser & Photonics Reviews* **2013**, *7*, 171-187.
- 11. Coppens, Z. J.; Li, W.; Walker, D. G.; Valentine, J. G., Probing and Controlling Photothermal Heat Generation in Plasmonic Nanostructures. *Nano Lett* **2013**, *13*, 1023-1028.
- 12. Groeneveld, R. H. M.; Sprik, R.; Lagendijk, A., Ultrafast Relaxation of Electrons Probed by Surface Plasmons at a Thin Silver Film. *Phys. Rev. Lett.* **1990**, *64*, 784-787.
- 13. Ganser, A.; Benner, D.; Waitz, R.; Boneberg, J.; Scheer, E.; Leiderer, P., Time-Resolved Optical Measurement of Thermal Transport by Surface Plasmon Polaritons in Thin Metal Stripes. *Appl Phys Lett* **2014**, *105*, 191119.
- 14. Möller, T. B.; Ganser, A.; Kratt, M.; Dickreuter, S.; Waitz, R.; Scheer, E.; Boneberg, J.; Leiderer, P., Fast Quantitative Optical Detection of Heat Dissipation by Surface Plasmon Polaritons. *Nanoscale* **2018**, *10*, 11894-11900.
- 15. Lundeberg, Mark B.; Gao, Y.; Woessner, A.; Tan, C.; Alonso-González, P.; Watanabe, K.; Taniguchi, T.; Hone, J.; Hillenbrand, R.; Koppens, F. H. L., Thermoelectric Detection and Imaging of Propagating Graphene plasmons. *Nature Materials* **2016**, *16*, 204.

- 16. Dombi, P.; Hörl, A.; Rácz, P.; Márton, I.; Trügler, A.; Krenn, J. R.; Hohenester, U., Ultrafast Strong-Field Photoemission from Plasmonic Nanoparticles. *Nano Lett* **2013**, *13*, 674-678.
- 17. Lehmann, J.; Merschdorf, M.; Pfeiffer, W.; Thon, A.; Voll, S.; Gerber, G., Surface Plasmon Dynamics in Silver Nanoparticles Studied by Femtosecond Time-Resolved Photoemission. *Phys. Rev. Lett.* **2000**, *85*, 2921-2924.
- 18. Rybka, T.; Ludwig, M.; Schmalz, M. F.; Knittel, V.; Brida, D.; Leitenstorfer, A., Sub-Cycle Optical Phase Control of Nanotunnelling in the Single-Electron Regime. *Nature Photonics* **2016**, *10*, 667.
- 19. Vogelsang, J.; Robin, J.; Nagy, B. J.; Dombi, P.; Rosenkranz, D.; Schiek, M.; Groß, P.; Lienau, C., Ultrafast Electron Emission from a Sharp Metal Nanotaper Driven by Adiabatic Nanofocusing of Surface Plasmons. *Nano Lett* **2015**, *15*, 4685-4691.
- 20. Harzheim, A.; Spiece, J.; Evangeli, C.; McCann, E.; Falko, V.; Sheng, Y.; Warner, J. H.; Briggs, G. A. D.; Mol, J. A.; Gehring, P., et al., Geometrically Enhanced Thermoelectric Effects in Graphene Nanoconstrictions. *Nano Lett* **2018**, *18*, 7719-7725.
- 21. Mennemanteuil, M.-M.; Colas-des-Francs, G.; Buret, M.; Dasgupta, A.; Cuadrado, A.; Alda, J.; Bouhelier, A., Laser-Induced Thermoelectric Effects in Electrically Biased Nanoscale Constrictions. In *Nanophotonics*, 2018; Vol. 7, p 1917.
- 22. Shi, S. F.; Xu, X.; Ralph, D. C.; McEuen, P. L., Plasmon Resonance in Individual Nanogap Electrodes Studied Using Graphene Nanoconstrictions as Photodetectors. *Nano Lett* **2011,** *11*, 1814-1818.

- Zolotavin, P.; Evans, C.; Natelson, D., Photothermoelectric Effects and Large
  Photovoltages in Plasmonic Au Nanowires with Nanogaps. *J Phys Chem Lett* 2017, 8, 1739-1744.
- 24. Szakmany, G. P.; Orlov, A. O.; Bernstein, G. H.; Porod, W., Single-Metal Nanoscale Thermocouples. *IEEE Trans. Nano.* **2014**, *13*, 1234-1239.
- 25. Zolotavin, P.; Evans, C. I.; Natelson, D., Substantial Local Variation of the Seebeck Coefficient in Gold Nanowires. *Nanoscale* **2017**, *9*, 9160-9166.
- 26. Fung, E. D.; Adak, O.; Lovat, G.; Scarabelli, D.; Venkataraman, L., Too Hot for Photon-Assisted Transport: Hot-Electrons Dominate Conductance Enhancement in Illuminated Single-Molecule Junctions. *Nano Lett* **2017**, *17*, 1255-1261.
- 27. Kornbluth, M.; Nitzan, A.; Seideman, T., Light-Induced Electronic Non-Equilibrium in Plasmonic Particles. *J. Chem. Phys.* **2013**, *138*, 174707.
- 28. Natelson, D.; Evans, C. I.; Zolotavin, P., *Photovoltages and Hot Electrons in Plasmonic Nanogaps*. SPIE: 2018; Vol. 10540.
- 29. Sundararaman, R.; Narang, P.; Jermyn, A. S.; Goddard Iii, W. A.; Atwater, H. A., Theoretical Predictions for Hot-Carrier Generation from Surface Plasmon Decay. *Nat. Comm.* **2014**, *5*, 5788.
- 30. Kumarasinghe, C. S.; Premaratne, M.; Bao, Q.; Agrawal, G. P., Theoretical Analysis of Hot Electron Dynamics in Nanorods. *Scientific Reports* **2015**, *5*, 12140.

- 31. Li, W.; Valentine Jason, G., Harvesting the Loss: Surface Plasmon-Based Hot Electron Photodetection. In *Nanophotonics*, 2017; Vol. 6, p 177.
- 32. Khurgin, J. B., Hot Carriers Generated by Plasmons: Where Are They Generated and Where Do They Go from There? *Faraday Discussions* **2019**.
- 33. Wu, S.; Sheldon, M. T., Optical Power Conversion Via Tunneling of Plasmonic Hot Carriers. *ACS Photonics* **2018**, *5*, 2516-2523.
- 34. Evans, C. I.; Zolotavin, P.; Alabastri, A.; Yang, J.; Nordlander, P.; Natelson, D., Quantifying Remote Heating from Propagating Surface Plasmon Polaritons. *Nano Lett* **2017**, *17*, 5646-5652.
- 35. Ghafoori, G.; Boneberg, J.; Leiderer, P.; Scheer, E., Tuning the Transmission of Surface Plasmon Polaritons across Nano and Micro Gaps in Gold Stripes. *Opt. Express* **2016**, *24*, 17313-17320.
- 36. Müller, M.; Kravtsov, V.; Paarmann, A.; Raschke, M. B.; Ernstorfer, R., Nanofocused Plasmon-Driven Sub-10 Fs Electron Point Source. *ACS Photonics* **2016**, *3*, 611-619.
- 37. Ropers, C.; Neacsu, C. C.; Elsaesser, T.; Albrecht, M.; Raschke, M. B.; Lienau, C., Grating-Coupling of Surface Plasmons onto Metallic Tips: A Nanoconfined Light Source. *Nano Lett* **2007**, *7*, 2784-2788.
- 38. Ittah, N.; Noy, G.; Yutsis, I.; Selzer, Y., Measurement of Electronic Transport through 1g0 Gold Contacts under Laser Irradiation. *Nano Lett* **2009**, *9*, 1615-1620.

- 39. Ittah, N.; Selzer, Y., Electrical Detection of Surface Plasmon Polaritons by 1g0 Gold Quantum Point Contacts. *Nano Lett* **2011**, *11*, 529-534.
- 40. Kolloch, A.; Benner, D.; Bädicker, M.; Waitz, R.; Geldhauser, T.; Boneberg, J.; Leiderer, P.; Scheer, E., *Characterization and Applications of Plasmon Fields in Metal Nanostructures*. SPIE: 2011; Vol. 8204.
- 41. Wang, X.; Evans, C. I.; Natelson, D., Photothermoelectric Detection of Gold Oxide Nonthermal Decomposition. *Nano Lett* **2018**, *18*, 6557-6562.
- 42. Zolotavin, P.; Alabastri, A.; Nordlander, P.; Natelson, D., Plasmonic Heating in Au Nanowires at Low Temperatures: The Role of Thermal Boundary Resistance. *ACS Nano* **2016**, *10*, 6972-6979.
- 43. Herzog, J. B.; Knight, M. W.; Natelson, D., Thermoplasmonics: Quantifying Plasmonic Heating in Single Nanowires. *Nano Lett* **2014**, *14*, 499-503.
- 44. Marschall, J.; Majumdar, A., Charge and Energy Transport by Tunneling Thermoelectric Effect. *J Appl Phys* **1993**, *74*, 4000-4005.
- 45. Reddy, P.; Jang, S.-Y.; Segalman, R. A.; Majumdar, A., Thermoelectricity in Molecular Junctions. *Science* **2007**, *315*, 1568.
- 46. Liu, Y.-S.; Chen, Y.-C., Seebeck Coefficient of Thermoelectric Molecular Junctions: First-Principles Calculations. *Phys Rev B* **2009**, *79*, 193101.
- 47. Ludoph, B.; Ruitenbeek, J. M. v., Thermopower of Atomic-Size Metallic Contacts. *Phys Rev B* **1999**, *59*, 12290-12293.

- 48. Wang, F.; Melosh, N. A., Plasmonic Energy Collection through Hot Carrier Extraction. *Nano Lett* **2011**, *11*, 5426-5430.
- 49. Evans, K. M.; Zolotavin, P.; Natelson, D., Plasmon-Assisted Photoresponse in Ge-Coated Bowtie Nanojunctions. *ACS Photonics* **2015**, *2*, 1192-1198.
- 50. Herzog, J. B.; Knight, M. W.; Li, Y. J.; Evans, K. M.; Halas, N. J.; Natelson, D., Dark Plasmons in Hot Spot Generation and Polarization in Interelectrode Nanoscale Junctions. *Nano Lett* **2013**, *13*, 1359-1364.

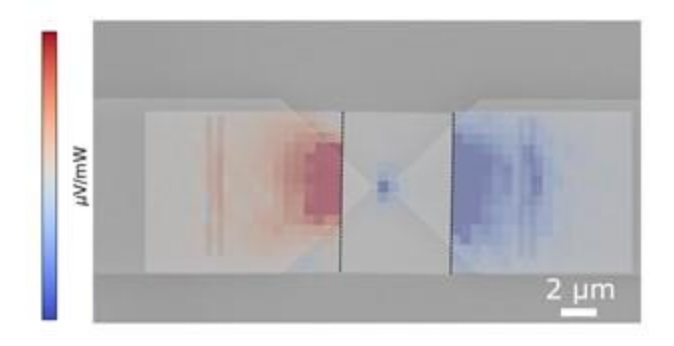


Table of Contents Graphic